Chemical Engineering Journal 498 (2024) 155260

Contents lists available at ScienceDirect

Chemical Engineering Journal

journal homepage: www.elsevier.com/locate/cej

Magnetic resonance velocimetry of thin falling films

Georges C. Saliba [a,*], Jan G. Korvink [a], Juergen J. Brandner [a,b]

[a] Institute of Microstructure Technology (IMT), Karlsruhe Institute of Technology (KIT), Hermann-von-Helmholtz-Platz 1, 76344 Eggenstein-Leopoldshafen, Germany
[b] Karlsruhe Institute of Technology, Karlsruhe Nano Micro Facility KNMFi, Hermann-von-Helmholtz-Platz 1, 76344 Eggenstein-Leopoldshafen, Germany

ARTICLE INFO

Keywords:
Falling films
Gas–liquid contactor
Hydrodynamics
Gas absorption

ABSTRACT

Falling film microreactors are a type of liquid–gas contactor based on a gravity-driven film flow. These devices achieve high interfacial areas per unit volume compared to other contactors. Nevertheless, they are limited by the liquid-side mass transfer. To overcome this issue, the operating conditions must be chosen in a way to enhance gas absorption and ensure efficient transfer within the film. The present study looks into the use of magnetic resonance velocimetry to study the velocity field inside of falling films at the microscale. Two parameters were considered, the channel geometry, and the volumetric flow rate. The aim was not only to determine the conditions that optimize the interfacial area, but also to showcase the capabilities and advantages of magnetic resonance velocimetry for this type of flow configuration. In addition, a straightforward mathematical model, based on the Navier–Stokes equations, is used to predict the thickness of the film, since previous approaches, mainly those of Kapitza and Nusselt, are not valid for flows at the microscale, where surface tension phenomena predominate. It was shown that the round channel yields by far the highest surface-to-volume ratio, twice as high as for the rectangular channel for the same volumetric flow rate. In addition, film breakup was not observed in the round channel even for volumetric flow rates of down to 0.27 mL min^{-1}.

1. Introduction

Falling films have been studied in the context of micro-reaction technology, with the aim of increasing the rate of absorption or conversion. In typical situations, viscous, inertial, and gravitational forces predominate, while surface tension is neglected. At the microscale, however, the balance of forces tips in favor of surface tension, which then directly affects the film, in particular the shape of its surface. The shape and surface area of the liquid/gas interface are determining factors for the rate of absorption of a given gas species into the liquid phase. Depending on the value of the contact angle at the three-phase point, the curved surface of the film can lead to an alteration of the velocity distribution by shifting the maximum velocity from the center of the microchannel towards the edges, as was noted by Anastasiou et al. [1] and Al-Rawashdeh et al. [2]. Since the velocity of the film at a given location depends on its depth, the curvature of the interface leads to an increase in velocity towards the edges of the channel. This effect is particularly prominent for rectangular channels, and can be suppressed by using channels without corners [2].

Liquid–gas contactors fall into two categories, those involving dispersion of one phase into the other, and those based on film flows, either gravity- or pressure-driven [3]. Falling film micro-reactors, involving gravity-driven film flows, have already been used to perform a wide range of reactions [4] such as fluorination [5], chlorination [6], sulfonation [7], and hydrogenation [8]. Nevertheless, many challenges persist in the design of these reactors. A recent survey on continuous-flow microreactors [9] compared different liquid–gas contacting techniques. In spite of the challenges related to scale-up, falling film microreactors stood out in terms of surface-to-volume ratio, in other words, they provided the largest relative contact surface between the liquid and gas phases. However, accurate predictions of performance are difficult to come by as was shown repeatedly in the literature [10]. The persistent use of models that were developed for macroscale flows is problematic, since they do not account for phenomena which are predominant at the microscale such as surface tension. In addition, the mass transport in the liquid phase is a bottleneck in improving falling film reactors. The liquid-side mass transfer rate can significantly impact the overall reaction rate, in particular when the reaction kinetics are faster than the mass transfer rate. Understanding and controlling the hydrodynamics of the flow is crucial for enhancing mass transfer and improving reactor performance. In this regard, most researchers in the field resort to numerical methods. Nevertheless, the potential to improve liquid-side mass transfer by understanding the flow and even controlling it remains unexploited.

Micro-channel falling films exhibit three distinct flow regimes. For low mass flow rates, the flow is restricted to the corners of the channel

* Corresponding author.
E-mail address: georges.saliba@kit.edu (G.C. Saliba).

https://doi.org/10.1016/j.cej.2024.155260
Received 9 July 2024; Received in revised form 8 August 2024; Accepted 27 August 2024
Available online 31 August 2024

and forms a rivulet pair leaving the central part of the channel dry. Upon increasing the mass flow rate, these rivulets swell until they come in contact with one another at certain points along the length of the channel. Dry patches appear and remain stable as long as surface tension at their boundary can balance the inertial force of the flow. Past a certain value of the mass flow rate, the dry patches disappear and the falling film is complete. The transition between these last two regimes has only been characterized using optical methods. For instance, Zhang et al. [11] illuminated the channel from the back with a cold fiber-optic lamp and imaged the flow using a high-speed CCD camera. In works such as Patel and Garimella [12], Yu et al. [13] or Anastasiou et al. [1], the shape of a liquid/gas interface for a complete was successfully measured using optical techniques. The same has not yet been done for the dry patches regime.

In addition to increasing the surface area of the interface, it is also desirable to minimize the volume to free surface ratio by reducing the thickness of the film while keeping it stable and free of dry patches. The critical mass flow rate needed to transition from the dry patches to the complete films regimes depends on the properties of the fluid, in particular surface tension. Zhang et al. [11] demonstrated that lowering the surface tension of water by mixing it with ether glycol reduces the threshold. A thin stable film can also be obtained by taking advantage of the hysteresis effect in the transition between the complete and dry patches regimes. Zhang et al. [11] demonstrated that once the complete flow is achieved, it is possible to lower the mass flow rate down to one eighth of the threshold required to transition from the dry patch regime to the complete film.

Measurements of the film thickness or velocity are usually obtained from optical techniques such as stereo digital microscopy [14], confocal laser scanning microscopy or laser profilometry [15]. The most widely used method, however, remains micro-Particle Image Velocimetry (microPIV) [1] and its variants which rely on injecting visible particles into the flow [16]. In spite of their wide usage, optical methods offer limited information on the flow and they require optical access which, as a consequence, is not appropriate liquid/gas interfaces with complex shapes. For instance, in measuring the curvature of the interface, stereo-digital microscopy [14] cannot reach the vicinity of the side walls since the inclined beam of light would be blocked by the corner of the open channel. Moreover, microPIV provides two-component velocity vectors in individual planes.

In sum, micro-falling films feature complex flow phenomena that need to be understood in order to better design efficient microreactors. One aim is to be able to produce very thin but stable films with a large (relative) open surface. To gain the necessary understanding, velocity measurements are needed in the entire film in its different regimes. Magnetic resonance velocimetry is a method which is gaining more traction in process engineering, as it provides a wealth of information on flow phenomena in a non-intrusive way, and without the need for optical access. As pointed out by Sobieszuk et al. [17], the hydrodynamics of falling films in open-channel microreactors has not received a lot of attention over the years. In a more recent review of the topic by Mohammed and Lokhat [10], a few studies are cited that use numerical tools such as CFD in order to further our understanding of flow behavior in FFMRs. Nevertheless, many questions remain unanswered with regards to flow phenomena at this scale. For instance, Sobieszuk et al. [18] showed that, in a microreactor, the absorption rate of CO_2 in a CO_2-Monoethylamine(MEA)-H_2O system was four times higher than in a CO_2 in a CO_2-NaOH-H_2O system. The same phenomenon occurs at larger scales and is attributed to the appearance of Marangoni cells due to surface tension inhomogeneities [19,20]. The authors then conclude that, in spite of the laminar nature of the flow and the sub-millimeter dimensions of the channel, Marangoni cells also appear at the micro-scale and improve absorption. However, these flow structures were not observed directly. Magnetic Resonance Velocimetry offers a non-invasive way to measure the flow inside the microfluidic system without the need for optical access. To our knowledge, no studies have been conducted on falling films using magnetic resonance since the work by Heine et al. [21]. They measured the semi-parabolic average velocity profile, which is a characteristic of laminar falling films. By increasing the Reynolds number, waves appear at the surface of the film and result in a different average velocity profile consisting of two overlapping parabolas.

In the field of chemistry, magnetic resonance is closely associated with the analysis of chemical compounds via Nuclear Magnetic Resonance. However, microreactor design can benefit greatly from magnetic resonance velocimetry by characterizing the flow inside the devices as it is varying, as opposed to studying the composition of the liquid after the absorption and reaction has taken place [22,23]. To study the flow and to explain enhancement, a large part of the literature is either based on hypotheses [18], numerical simulations [2,24,25], or film thickness measurements [13,14,26]. Investigators have also used micro-particle image velocimetry [1,16] to measure velocity fields, although defocusing and the presence of a curved interface in the light path constitute hurdles to measuring the velocity accurately. To better understand what goes on inside a falling film microreactor, more focus should be given to the fluid dynamics of the problem, and this is afforded by using magnetic resonance velocimetry which gives both detailed spatio-temporal, and compositional, information about the flow. Compared to traditional techniques, there are a number of constraints inherent to magnetic resonance velocimetry, such as the limited space available for the flow setup, and the magnetic field compatibility of the materials used. Nevertheless, in the case of microfluidic systems like the ones we study in this work, these are not issues since the setup has dimensions on the scale of a few millimeters and the parts are 3D-printed with non-magnetic materials. In addition, the workflow of performing MRV can be streamlined so that it becomes a powerful tool for experimental fluid mechanics. Post-processing is particularly simple, as velocity fields are directly obtained, right after the experiment is done. In the case of PIV-based techniques, the images taken during the experiment have to be processed in order to detect and track the particles in the flow, only to then deduce the velocity field. One of the aims of this work is then to demonstrate the wealth of information that can be extracted from the flow and the ability of MRV, to characterize a canonical flow, namely, a vertical open-channel flow having sub-millimeter dimensions.

The present study uses four different channel geometries to produce falling films at different volumetric flow rates. The downwards velocity component was measured in the cross-sectional plane of the films. The data was also used to deduce the minimum thickness of the film as well as the surface-to-volume ratio. A mathematical model, obtained by simplifying the Navier–Stokes equations, was used to predict the thickness of the film and compared to classical expressions for the thickness proposed by Nusselt, and Kapitza, respectively.

2. Materials and methods

Experimental setup

Distilled water is used as a working fluid for all of the measurements. The experiments were conducted inside an 11.7 T nuclear magnetic resonance system (Bruker BioSpin) with a ^{1}H resonance frequency of 500 MHz, as illustrated in Fig. 1. The 3D-printed flow cell was made by stereolithography and is shown in Fig. 2. In magnetic resonance experiments, radio-frequency coils are typically designed to accommodate standard-sized test tubes containing chemicals. Consequently, probe heads are not usually intended for flow experiments and offer very limited space. A Micro 5 MR microscopy probe, with a maximum field gradient of 3 T m^{-1}, was used. This probe features a 10 mm receiver/transmitter saddle coil supported on glass mounts. The inner volume of the coil was accessible only from the top side, preventing setting up a flow-through experiment.

To meet these constraints, a microreactor was designed so that both its inlet and outlet were connected on top. The microreactor consisted

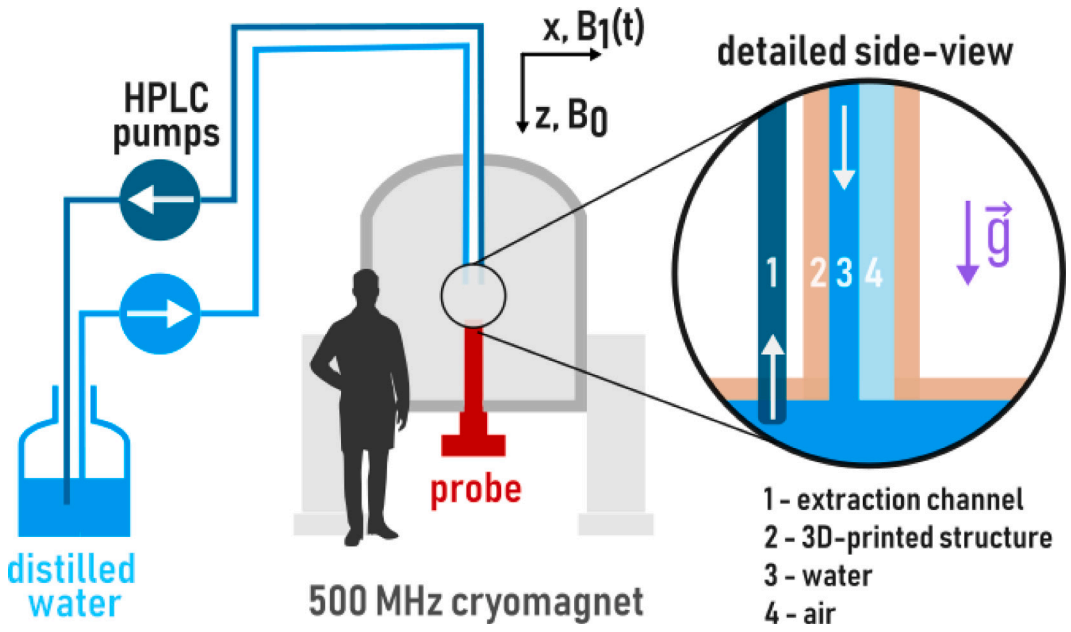

Fig. 1. Illustration of the experimental setup. On the right, a detailed cross-sectional view of the open-channel is presented.

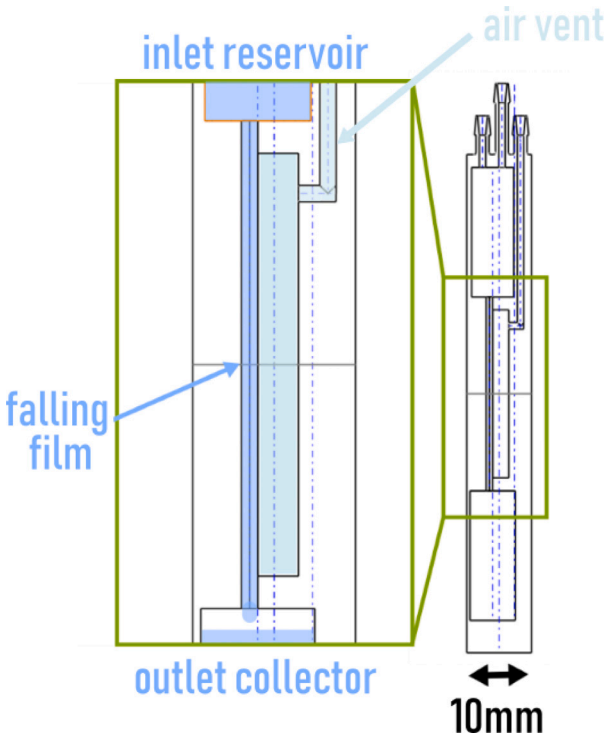

Fig. 2. 3D-printed flow cell used for the experiments.

of an open channel, which was fed from a reservoir to ensure steady inlet conditions. Downstream, the water accumulated in a sump and was pumped out. A venting channel was added to maintain atmospheric pressure in the gas phase. Four different parts having rectangular, angled, and curved channels were investigated, in order to ascertain the effect of channel geometry on velocity distribution and film thickness. Two identical HPLC pumps from Knauer (KNAUER 40P, Berlin, Germany), with 10 mL min^{-1} pump heads, were used for feeding and extracting the distilled water.

Magnetic resonance velocimetry

A common method to measure velocity using NMR is to encode the motion in the phase of the spin ensemble. Spin ensembles act as magnetic moments, and as they travel through a magnetic field gradient, they experience a precession phase shift. It can be shown that, if the gradient field is linear in space, the phase shift is proportional to velocity along the direction of the gradient The advantage of this technique is that the velocity of the fluid particles (or their protons) is measured directly, unlike hot-wire velocimetry where the probe can disturb the flow, or PIV which actually measures the speed of the seeding particles and not the fluid itself.

To measure velocity and obtain signals from spin ensembles in NMR, a specific pulse sequence is needed. It usually includes a radio-frequency pulse combined with precisely timed applied magnetic field gradients in the x, y, and z directions. These actions create a radio-frequency echo from the sample, which is then measured and analyzed. The overlapping parts of these sequences allow for operations such as slice selection (choosing the measurement plane), velocity encoding, and k-space sampling for spatial location.

In this study, we used the "FLOWMAP" sequence (ParaVision 6.0.1, Bruker BioSpin MRI GmbH, Ettlingen, Germany), a standard Cartesian 4D MRV sequence. This method combines a 3D gradient-echo with a 4-point Hadamard velocity encoding scheme [27]. The spatial resolution is 20 µm in the x- and y-directions. The results are averaged on a 2 mm thick section of the flow in the z-direction. An RF pulse is sent into the sample, causing the spins — affected by a strong magnetic field — to emit an echo that the RF coil detects. In MR velocimetry, the response of the sample depends on the strength and distribution of the magnetic field, which is controlled by magnetic gradient coils. By adjusting the gradients' strength and timing along three axes, spatial and velocity information is encoded into the spins for measurement. A short presentation of how velocity is encoded can be found in Saliba et al. [28], and for a more expansive treatment, the reader is referred to specialized texts on the topic of magnetic resonance velocimetry such as Fukushima [29], Elkins and Alley [30] or Bernstein et al. [31].

Regarding post-processing, MRV offers an additional advantage over PIV in that the velocity maps are obtained directly after the experiment is done. The measured signals undergo a Fourier transform which results in a spatial distribution of the three components of the velocity vector. Further processing is performed in MATLAB to obtain secondary

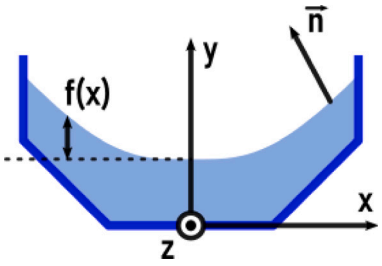

Fig. 3. Diagram of the mathematical model developed in the present section. The darker contour represents the channel walls.

quantities, such as the surface-to-volume ratio of the film, the shear stress at the interface, or the volume flow rate.

Mathematical model

The mathematical model developed in this section is diagrammed in Fig. 3. The Navier–Stokes equations,

$$\frac{\partial u}{\partial t}+u\frac{\partial u}{\partial x}+v\frac{\partial u}{\partial y}+w\frac{\partial u}{\partial z}=-\frac{1}{\rho}\frac{\partial p}{\partial x}+\nu\left(\frac{\partial^2 u}{\partial x^2}+\frac{\partial^2 u}{\partial y^2}+\frac{\partial^2 u}{\partial z^2}\right)+f_x \quad (1)$$

$$\frac{\partial v}{\partial t}+u\frac{\partial v}{\partial x}+v\frac{\partial v}{\partial y}+w\frac{\partial v}{\partial z}=-\frac{1}{\rho}\frac{\partial p}{\partial y}+\nu\left(\frac{\partial^2 v}{\partial x^2}+\frac{\partial^2 v}{\partial y^2}+\frac{\partial^2 v}{\partial z^2}\right)+f_y \quad (2)$$

$$\frac{\partial w}{\partial t}+u\frac{\partial w}{\partial x}+v\frac{\partial w}{\partial y}+w\frac{\partial w}{\partial z}=-\frac{1}{\rho}\frac{\partial p}{\partial z}+\nu\left(\frac{\partial^2 w}{\partial x^2}+\frac{\partial^2 w}{\partial y^2}+\frac{\partial^2 w}{\partial z^2}\right)+f_z, \quad (3)$$

can be simplified by assuming that the velocity has a single component and that the flow is steady and fully developed, i.e., $\vec{V}=w(x,y)\vec{e}_z$, $u=v=0$, and the only body force is gravity $\vec{f}=\vec{g}=g\vec{e}_z$. The simplified equations become

$$0=\partial_x p, \quad (4)$$

$$0=\partial_y p, \quad (5)$$

$$0=\nu\partial_{xx}w+\nu\partial_{yy}w+g, \quad (6)$$

As mentioned in the introduction, surface tension has a significant role in the present configuration, and manifests itself through the curvature of the free surface:

$$\kappa=\frac{f''(x)}{\left(1+f'(x)^2\right)^{3/2}}, \quad (7)$$

where f is the height of the film in the y-direction, measured from the bottom of the meniscus, as illustrated in Fig. 3. The curvature of the meniscus also determines the pressure at the free surface:

$$p=\sigma\kappa. \quad (8)$$

In addition, the kinematic boundary condition at the free surface $\vec{V}\cdot\vec{n}$ is always satisfied in the present case since $\vec{V}=w(x,y)\vec{e}_z$. Finally, the no-slip condition $\vec{V}=\vec{0}$ is applied at the channel walls.

Combining Eqs. (5), (7) and (8), the following differential equation can be found for the height f of the film:

$$f'''f'^2-3f''^2f'+f'''=0. \quad (9)$$

The boundary conditions at the contact line are dictated by the contact angle θ, such that $f'(\pm x)=\pm\cot(\theta)$, and assuming the film is symmetrical about the y-axis, the second derivative of f must be zero at $x=0$, i.e., $f''(0)=0$. The differential equation for f is solved numerically using the finite element method. The shape of the interface is then used, along with the channel geometry, to define the domain over which the Poisson Eq. (6) is solved. Assuming once more that the film is symmetrical about the y-axis, only half the film needs to be resolved, with a zero-gradient boundary condition along y. A no-slip boundary condition is imposed along the walls, and a von Neumann condition at the interface:

$$\vec{n}\cdot\vec{\nabla}w=G(x,y), \quad (10)$$

where $\vec{n}$ is the vector normal to the interface. If it is assumed that shear stress at the interface is negligible, the von Neumann boundary condition function $G(x,y)$ can be set to zero. This problem is solved numerically using the finite-element method to obtain the velocity distribution inside the liquid film.

In addition to providing velocity fields for different channel shapes and volumetric flow rates, the analytical model can be used to predict the thickness of the film. The classical approaches proposed by Nusselt and later on by Kapitza are still widely used to evaluate results, both numerical and experimental. Nusselt suggested a model predicated on a balance between shear and gravitational forces:

$$\frac{d}{dx}\tau_{xz}=\rho g, \quad (11)$$

in order to determine the film thickness. It was also assumed that the shear stress at the liquid–air interface is negligible and that the flow is laminar. This resulted in the following expression for the film thickness:

$$\delta_{\mathrm{Nu}}=\left(\frac{3Q\mu}{w\rho g}\right)^{1/3}. \quad (12)$$

Although neglecting shear stress from the gas phase remains a reasonable assumption in open microchannels, surface tension can no longer be set aside. Depending on contact angle, the surface tension can cause the interface to deform in a drastic way, increasing the surface-to-volume ratio of the film. In spite of this over-simplification, this model is still being used to evaluate falling film flows at the microscale.

Kapitza developed a more elaborate model which incorporated surface undulations. At the time, experiments showed that waves could appear for Reynolds numbers as low as 20, which is well within the typical laminar flow regime. Where Nusselt only considered a balance between shear forces and viscous forces, Kapitza included both surface tension and a body force, namely, gravity. He demonstrated that the average thickness of an undulating film is less than that of a laminar film having the same flow rate Q. He showed that the potential energy of the film is equal to $(1/2)a_0x_0^2\ g\rho$ where a_0 is the average film thickness. At equilibrium, the most stable state is that which minimizes the potential energy. In the case of a falling film, the undulating state would have a lower potential energy than a laminar state owing to its lesser average thickness. The expression for average film thickness was found to be:

$$\delta_{\mathrm{Ka}}=\left(\frac{2.4Q\mu}{w\rho g}\right)^{1/3}, \quad (13)$$

which is similar to the result obtained by Nusselt, except for the factor of 2.4.

In both the Nusselt and Kapitza approaches, the presence of the side walls is neglected, which is justifiable at the scales they considered. However, for microfluidic open channels, depending on the contact angle of the liquid on the side walls, the gas–liquid interface is noticeably curved, which affects the velocity distribution inside the film as well as its thickness. In spite of that, these expressions for the film thickness are still in wide use even in the context of microflows [1,14,26]. The model presented above accounts for surface tension as well as the possible effects of shear stress at the interface, by including $G(x,y)$.

3. Results and discussion

Velocity field

In this section, we take a look at the velocity field inside the liquid film for four different channel geometries, rectangular, chamfered, round, and wedge. At the scale studied here, surface tension affects

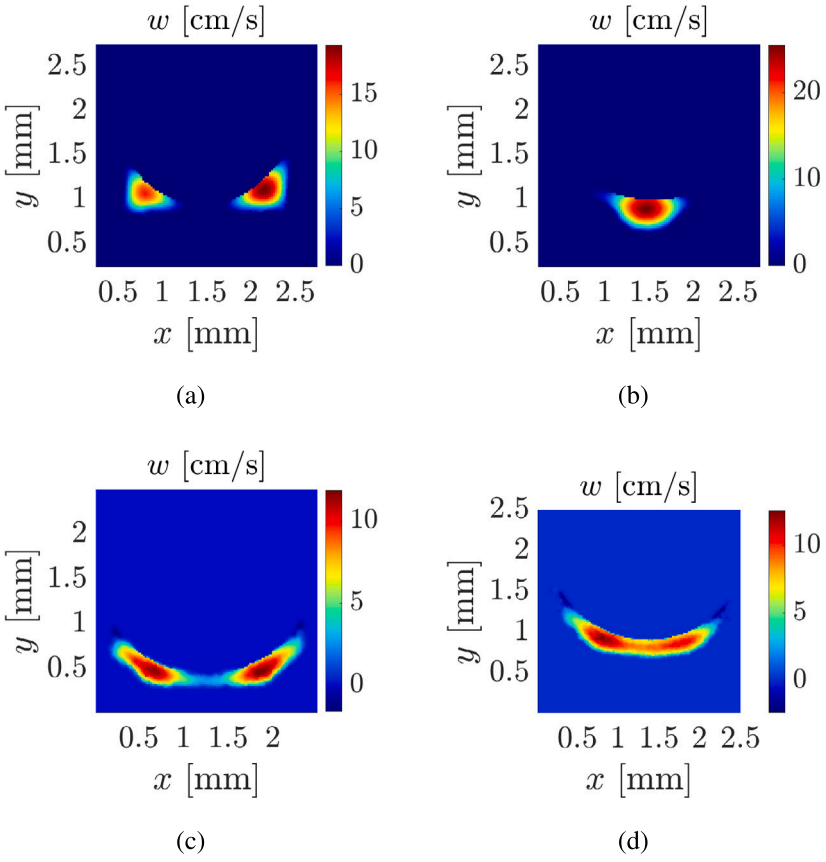

Fig. 4. Experimentally measured velocity fields $w(x, y)$ for 4(a) rectangular ($2.28\,\mathrm{mL\,min^{-1}}$), 4(b) wedge ($2.27\,\mathrm{mL\,min^{-1}}$), 4(c) chamfered ($1.85\,\mathrm{mL\,min^{-1}}$), and 4(d) round ($1.97\,\mathrm{mL\,min^{-1}}$) channel geometries.

the entire gas–liquid interface. The velocity profile in the y-direction is influenced by the thickness of the film at a given x position. For this reason, the maximum velocity does not occur in the middle of the film, rather, it is displaced towards the edge of the channel. For instance, this can be seen in Fig. 4(c) for the channel with chamfered corners. Al-Rawashdeh et al. [2] showed that only rectangular and isotropically-etched (rounded corner rectangle) channel shapes led to M-shaped velocity profiles. In the present case, due to imperfections in manufacturing the channels, the round geometry also had two velocity peaks, since the bottom of the channel was slightly flattened. This case is then comparable to a certain extent to the etched case in Al-Rawashdeh et al. [2]. The only configuration with a single maximum was the wedge-shaped channel (Fig. 4(b)). The rivulet regime could only be attained for the chamfered and rectangular geometries (see Fig. 4(a) for the rivulet regime in the rectangular channel) whereas the film in the wedge and round channels remained unbroken for the range of mass flow rates considered here.

Anastasiou et al. [1] found that the velocity profile under the meniscus along the width of the film, below the meniscus, has an M-shape if the ratio of the meniscus height to the film thickness is greater than one. Otherwise, the profile is parabolic. Figs. 5–7 show the velocity profiles along the tangent to the meniscus from the side wall to the center of the channel. In accordance with the observations made by Anastasiou et al. [1], the peak velocity does not occur at the center of the channel since the ratio of the meniscus height to film thickness remained greater than one.

In the case of the rectangular channel (Fig. 5), the velocity at the center of the channel decreased with mass flow rate until reaching zero just before film break-up. A similar observation could be made of the round channel Fig. 7, although film break-up was not reached for the lowest mass flow rate considered here. However, the velocity around the center of the chamfered channel became negative just before the onset of break-up. Velocity in the center was around $-1\,\mathrm{cm\,s^{-1}}$, whereas the maximum velocity reached $3\,\mathrm{cm\,s^{-1}}$.

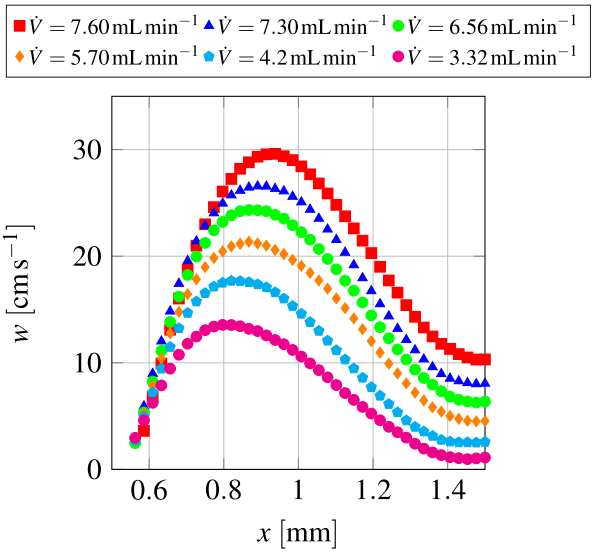

Fig. 5. Velocity profiles along the line tangent to the bottom of the meniscus for the rectangular open channel. Film break-up occurs for volumetric flow rates lower than $\dot{V} = 3.32\,\mathrm{mL\,min^{-1}}$.

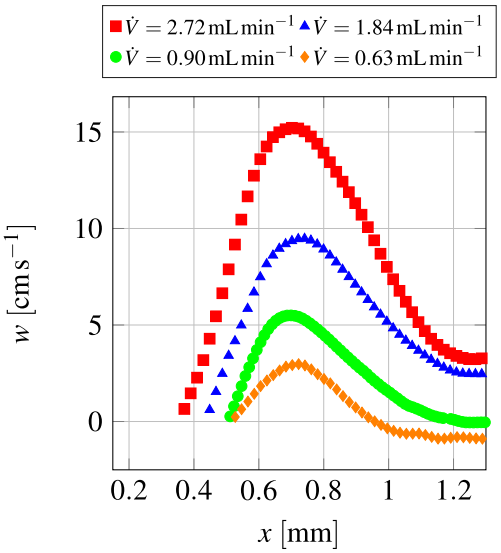

Fig. 6. Velocity profiles along the line tangent to the bottom of the meniscus for the chamfered open channel. Film break-up occurs for volumetric flow rates lower than $\dot{V} = 0.63\,\mathrm{mL\,min^{-1}}$.

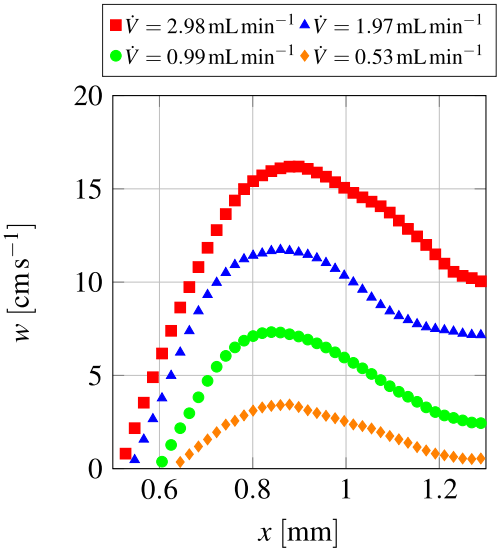

Fig. 7. Velocity profiles along the line tangent to the bottom of the meniscus for the round open channel. Film break-up does not occur for the range of volumetric flow rates considered in this study.

Film thickness

Unlike most other studies on micro-falling films [1,32,33], we chose to focus on the thickness distribution of the films rather than their height. The thickness τ is defined here as the distance between a set point and the closest point to it *across* the film. An example of thickness distribution along the entire contour of the film is presented in Fig. 8 for the round channel at $\dot{V} = 0.53\,\mathrm{mL\,min^{-1}}$. This definition of thickness reflects the diffusion-driven transport of the absorbed gas through the film, and avoids skew projections which tend to exaggerate the distance to a specific flow feature. The values of the thickness for each configuration was then plotted against position in Fig. 9. In the case of the rectangular channel, break-up occurred for an elevated value of the volumetric flow rate compared to the remaining geometries, which led us to consider flow rates greater than $3\,\mathrm{mL\,min^{-1}}$ for this channel shape.

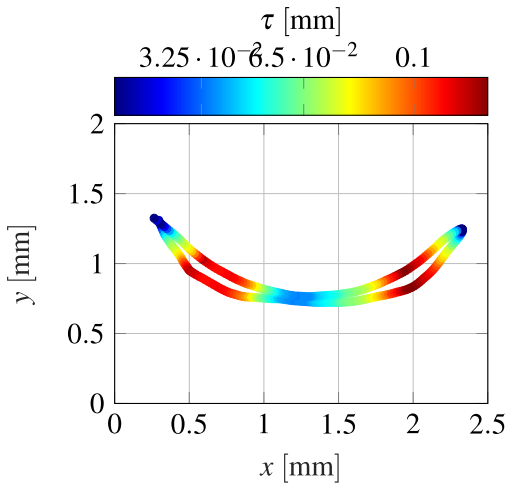

Fig. 8. Thickness of the film inside a circular open channel, which is defined as the shortest distance between a given point on the contour of the film, and a point facing it across the film.

For the remaining cases, the volumetric flow rate ranged from 0.22 to about $3\,\mathrm{mL\,min^{-1}}$. The four geometries result in a qualitative difference in thickness distribution, with round channels providing the flattest distribution over most of the film, before the film tapers off at the three-phase contact point. This is because both the meniscus and the bottom of the channel are curved and so maintain a relatively unchanging distance from one another, compared to the rectangular and chamfered geometries. In the latter two, the presence of corners results in significant increase of the thickness of the film compared to the minimum thickness at the center. For the wedge geometry, the liquid puddles up in the center of the channel resulting in an uneven thickness distribution across the film. Also worth noting is that, for nearly the same volumetric flow rate, the film is thicker at the center for the round channel as it is for the chamfered or rectangular ones. For instance, at $\dot{V} = 2.98\,\mathrm{mL\,min^{-1}}$, the thickness of the round film is 276 μm compared to 245 μm for the chamfered film at $\dot{V} = 2.72\,\mathrm{mL\,min^{-1}}$ and 180 μm for the rectangular film at $\dot{V} = 3.32\,\mathrm{mL\,min^{-1}}$. However, for the round film, this minimum thickness is maintained over most of the width of the channel, whereas for the remaining cases, it rapidly increases further away from the center.

Prediction of film thickness using the mathematical model

As a first assumption, the interfacial shear stress was set to zero since the viscosity of air is weak compared to that of water. However, as was already noted in the literature, the shear stress at a gas–liquid interface is not always negligible. To keep the model simple, a uniform value of −1000 was chosen for the von Neumann condition at the interface, i.e., $G(x, y) = G = -1000\,\mathrm{s^{-1}}$. This value is close to the average value of the gradient at the interface for the cases studied here. Therefore, with this parameter set to a constant, and the contact angle set to 50°, it was possible to obtain the velocity field and the minimum film thickness simply by specifying the volume flow rate. Results for the rectangular and chamfered channels are summarized in Table 1. The error is defined as the difference between the analytical and experimental values divided by the experimental values. For the rectangular case, the thickness of the film at its geometrical center is reported down to the lowest volumetric flow rate for which a stable complete film can be maintained. The analytical model, in spite of the fixed uniform value of g, predicts the value of the thickness with a relative error of 11% or less.

However, the experimental results can be corrected to account for the partial volume effect, which is a common artefact in MR imaging.

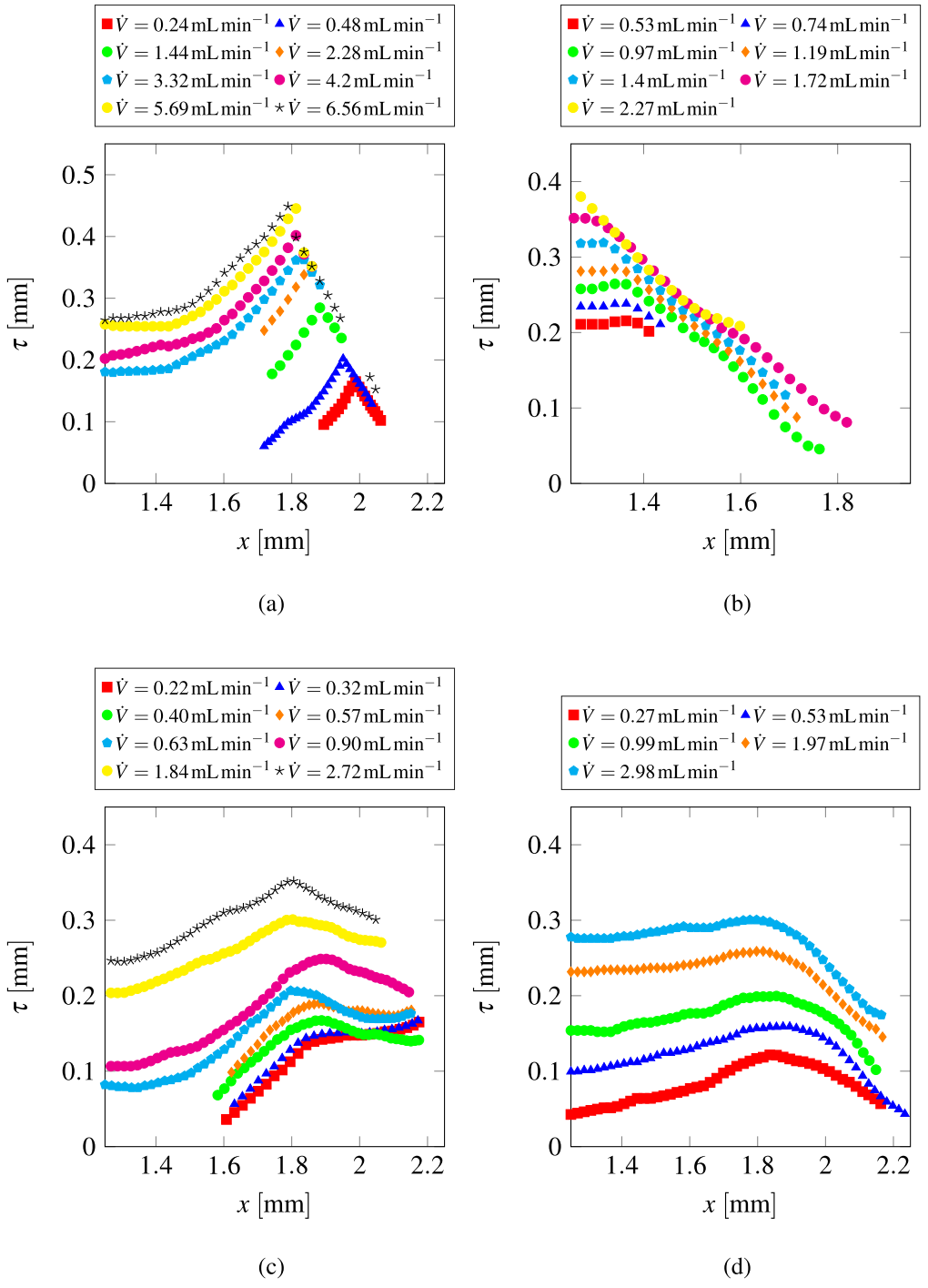

Fig. 9. Thickness distribution across thin falling films inside (a) rectangular, (b) wedge, (c) chamfered, and (d) round open channels.

When a boundary between two contrasting parts, here between liquid and gas, cuts through a pixel, it results in that pixel containing a non-zero value although it only partly contains a liquid. In other words, unless the boundary of the film coincides with the edges of a given pixel, the position of that boundary appears to be shifted outwards from the film. This results in an overestimation of the thickness of the film by half a pixel size on average. Taking the partial volume effect into consideration, the error is reevaluated and reported in the last column of Table 1. The predictions are then within 6% or less of the experimental results. The analytical model also predicts to within 6% the film thickness for the chamfered geometry. However, the accuracy quickly deteriorates when nearing film break-up, as can be seen for $\dot{V} = 0.90\,\mathrm{mL\,min^{-1}}$. The reason is, that the model assumes that the meniscus has the same shape regardless of the minimum thickness of the film. As the film approaches break-up, the fluid starts to separate into the corners of the channels, deforming the meniscus. This is not taken into account by the model. Nevertheless, the model predicts film thickness sufficiently accurately for higher volumetric flow rates.

For comparison, the thickness of the film was also found from the widely-used expression proposed by Nusselt, and Kapitza, respectively. The errors with respect to the corrected experimental results are presented in the last two columns for the rectangular channel. The Nusselt solution produces accurate estimations for high volumetric flow rates, but quickly falls through for lower ones reaching up to 16.3%. Although the expression found by Kapitza provides better estimations, it is still less accurate than the approach presented here.

Table 1
The minimal thickness of the film as a function of volume flow rate for different channel geometries. The errors that result from applying Nusselt's and Kapitza's models are included for comparison.

Channel	VFR (mL min^{-1})[a]	Experimental[b] (μm)	Analytical (μm)	Error (%)	Error, PVE[c] (%)	Error Kapitza	Error Nusselt
Rectangular	6.56	256	240	6.3	−1.8	−6.6	0.6
	5.69	248	222	10.5	−6.1	−7.9	−0.8
	4.20	200	188	6.0	−0.3	4.4	12.4
	3.32	180	160	11.1	−5.0	8.0	16.3
Chamfered	2.72	245	253	3.3	−1.4		
	1.84	202	225	11.4	−5.7		
	0.90	106	187	76.4	−65		
Round	2.98	275	253	8.4	5.0		
	1.97	234	213	10	6.0		
	0.99	154	156	0.7	−6.2		
	0.53	99	113	−5.6	−17		

[a] Volumetric flow rate.
[b] Without partial volume effect correction.
[c] Taking into account partial volume effect.

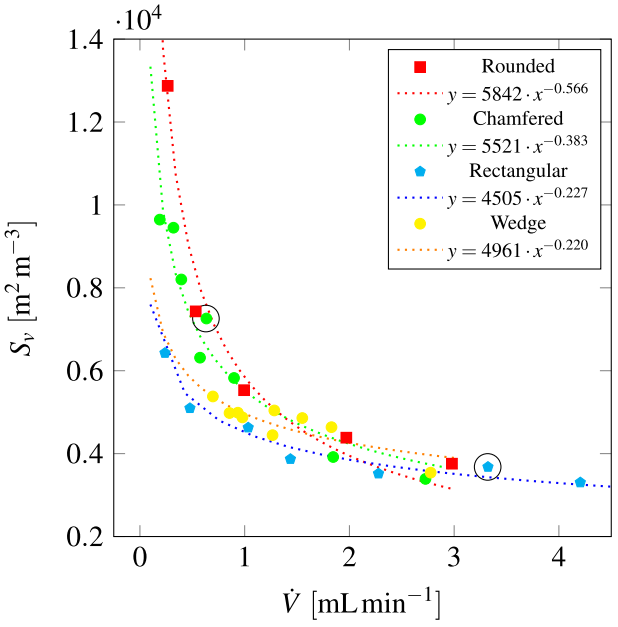

Fig. 10. Surface-to-volume ratio S_v as a function of volumetric flow rate for four different channel geometries with corresponding trend lines.

For the round channel, experimental measurements indicated that the film's edges were pinned at the channel corners. Consequently, the model was adjusted to reflect this pinning. The contact angle at the pinned edges varied, leading to changes in volumetric flow rates and film thicknesses. The error margin was around 6% or less, except for the lowest volumetric flow rate. This discrepancy is likely due to meniscus deformation, as can be deduced from Figs. 7 and 9(d). In Fig. 7, at a volumetric flow rate of 0.53 mL min^{-1}, the velocity under the center of the meniscus approaches zero. Fig. 9(d) reveals that the film thickness decreases towards the center. For higher flow rates, the thickness profile was relatively flat. These observations suggest the onset of film break-up, making the model invalid. Results for the wedge geometry were omitted due to significant discrepancies between experimental and analytical outcomes.

Surface-to-volume ratio

The mass transfer rate of a gas into a liquid phase can be informed by the volumetric mass transfer coefficient $k_L a$, which is defined as:

$$k_L a = \frac{A}{V} k_L \tag{14}$$

where a is the surface-to-volume ratio, A is the area of the interface, V is the volume of the liquid, and k_L the mass transfer coefficient based on liquid concentration. Increasing k_L or the ratio A/V enhances $k_L a$. The viscosity of the liquid, the diffusivity of the gas, and the liquid–gas affinity, all have an impact on the value of k_L. These factors cannot be tuned freely since they can depend on the reagents. However, the surface-to-volume ratio a can be improved by changing the shape of the channel. The surface-to-volume ratios were deduced from the velocity maps and are shown in Fig. 10. For the chamfered and rectangular channels, the lowest volumetric flow rate for which a stable film is maintained is indicated by a circle. Although the surface-to-volume ratio for the round channel was comparable to that of the other configurations for volumetric flow rates greater than 1 mL min^{-1}, it rapidly surpassed the others, reaching 12 871 m^2 m^{-3} for $\dot{V} = 0.27$ mL min^{-1} whereas the chamfered channel reached 9645 m^2 m^{-3} for $\dot{V} = 0.19$ mL min^{-1} and the rectangular channel 6427 m^2 m^{-3} for $\dot{V} = 0.24$ mL min^{-1}. In other words, with the round channel, it was possible to double the surface-to-volume ratio compared to a rectangular channel for nearly the same volumetric flow rate.

4. Conclusions

Microscale falling water films were investigated using magnetic resonance velocimetry. Liquid–gas interfaces are usually avoided at all costs in measurement techniques based on nuclear magnetic resonance since material susceptibility jumps provoke distortions in the B_0 magnetic field. However, with falling films, when the interface is arranged parallel to the magnetic field, it is possible to measure the flow in a completely non-intrusive way, unlike all other methods used in the literature so far.

Different geometries were considered, at a variety of volumetric flow rates, in order to obtain a film flow as thin and uniform as possible. The surface-to-volume ratio was computed as a measure for the intensity of mass transfer through the interface. It was shown that, in a round channel, the film does not break up at low volumetric flow rates, and that it reaches a surface-to-volume ratio almost twice as high as in a rectangular channel. The Navier–Stokes equations were simplified and solved numerically in order to predict the thickness of the flowing film. The model resulted in accurate predictions for rectangular, round, and chamfered channels, until the onset of film break-up. At this stage, the meniscus was deformed and the equation used to describe the shape of the interface was no longer valid. Finally, it was shown that, of the four geometries investigated, the round channel yielded the highest surface-to-volume ratio. For the lowest volumetric flow rate considered, the surface-to-volume ratio for the round channel was 33% and 100% higher than the chamfered and rectangular channels, respectively.

Magnetic resonance velocimetry is a suitable tool for studying falling films. Although this study focused on single-component flow, the

technique is capable of producing three-dimensional, three-component velocity fields necessary for examining flow within micro-structured channels. The prerequisites are sufficient spin polarization in the sample, and sufficient signal-to-noise ratio for the spin detection. On the other hand, a detailed understanding of the flow dynamics is crucial for the design of more efficient falling-film micro-reactors.

The results of our contribution will have relevance for the design of more efficient liquid–gas contactors, as used in biological applications as part of perfusion systems, and high-yield micro-reactors that benefit from microscale effects to achieve their stochiometric goals.

CRediT authorship contribution statement

Georges C. Saliba: Writing – original draft, Visualization, Methodology, Investigation, Conceptualization. **Jan G. Korvink:** Writing – review & editing, Supervision, Funding acquisition. **Juergen J. Brandner:** Writing – review & editing, Supervision, Funding acquisition.

Declaration of competing interest

The authors declare that they have no known competing financial interests or personal relationships that could have appeared to influence the work reported in this paper.

Data availability

Data will be made available on request.

Acknowledgments

GCS and JGK acknowledge partial funding through the ERC Synergy, Germany Grant No. 951459 (HiSCORE). JJB and JGK acknowledge support from the DFG, Germany for funding the CRC 1527 (HyPERiON). JJB and GCS acknowledge partial support of the Karlsruhe Nano Micro Facility (KNMFi), Germany, a Helmholtz Research Infrastructure at the Karlsruhe Institute of Technology. All authors acknowledge support by the KIT Publication Fund of the Karlsruhe Institute of Technology, Germany.

References

[1] A.D. Anastasiou, A. Gavriilidis, A.A. Mouza, Study of the hydrodynamic characteristics of a free flowing liquid film in open inclined microchannels, Chem. Eng. Sci. 101 (2013) 744–754.

[2] M. Al-Rawashdeh, A. Cantu-Perez, D. Ziegenbalg, P. Löb, A. Gavriilidis, V. Hessel, F. Schönfeld, Microstructure-based intensification of a falling film microreactor through optimal film setting with realistic profiles and in-channel induced mixing, Chem. Eng. J. 179 (2012) 318–329.

[3] C. de Bellefon, Gas–liquid-phase reactions: Addition, in: Micro Process Engineering, John Wiley & Sons, Ltd, 2009, pp. 143–165 (Chapter 26), URL https://onlinelibrary.wiley.com/doi/abs/10.1002/9783527631445.ch26.

[4] C.J. Mallia, I.R. Baxendale, The use of gases in flow synthesis, Org. Process Res. Dev. 20 (2) (2016) 327–360, http://dx.doi.org/10.1021/acs.oprd.5b00222.

[5] K. Jähnisch, M.P.D. Baerns, V. Hessel, W. Ehrfeld, V. Haverkamp, H. Löwe, C. Wille, A.E. Guber, Direct fluorination of toluene using elemental fluorine in gas/liquid microreactors, J. Fluor. Chem. (2000).

[6] H. Ehrich, D. Linke, K. Morgenschweis, M. Baerns, K. Jähnisch, Application of microstructured reactor technology for the photochemical chlorination of alkylaromatics, CHIMIA 56 (11) (2002) 647.

[7] T. Xie, C. Zeng, C. Wang, L. Zhang, Preparation of methyl ester sulfonates based on sulfonation in a falling film microreactor from hydrogenated palm oil methyl esters with gaseous SO3, 2013.

[8] K.K. Yeong, A. Gavriilidis, R. Zapf, V. Hessel, Experimental studies of nitrobenzene hydrogenation in a microstructured falling film reactor, Chem. Eng. Sci. 59 (2004) 3491–3494.

[9] A.A.H. Laporte, T.M. Masson, S.D.A. Zondag, T. Noël, Multiphasic continuous-flow reactors for handling gaseous reagents in organic synthesis: Enhancing efficiency and safety in chemical processes, Angew. Chem. 136 (11) (2024) e202316108.

[10] A.A. Mohammed, D. Lokhat, Mass transfer in falling film microreactors: measurement techniques and effect of operational parameters, Rev. Chem. Eng. 37 (2021) 277–303.

[11] H. Zhang, J. Yue, G. Chen, Q. Yuan, Flow pattern and break-up of liquid film in single-channel falling film microreactors, Chem. Eng. J. 163 (2010) 126–132.

[12] R.S. Patel, S.V. Garimella, Technique for quantitative mapping of three-dimensional liquid-gas phase boundaries in microchannel flows, Int. J. Multiph. Flow 62 (2014) 45–51.

[13] D. Yu, X. Hu, C. Guo, T. Wang, X. Xu, D. Tang, X. Nie, L. Hu, F. Gao, T. Zhao, Investigation on meniscus shape and flow characteristics in open rectangular microgrooves heat sinks with micro-PIV, Appl. Therm. Eng. 61 (2013) 716–727.

[14] Y. Yang, T. Zhang, D. Wang, S. Tang, Investigation of the liquid film thickness in an open-channel falling film micro-reactor by a stereo digital microscopy, J. Taiwan Inst. Chem. Eng. 98 (2019) 27–36.

[15] K.K. Yeong, A. Gavriilidis, R. Zapf, H.J. Kost, V. Hessel, A. Boyde, Characterisation of liquid film in a microstructured falling film reactor using laser scanning confocal microscopy, Exp. Therm Fluid Sci. 30 (2006) 463–472.

[16] A.T. Koupa, Y.G. Stergiou, A.A. Mouza, Free-flowing shear-thinning liquid film in inclined μ-channels, Fluids 4 (2019).

[17] P. Sobieszuk, J. Aubin, R. Pohorecki, Hydrodynamics and mass transfer in gas-liquid flows in microreactors, Chem. Eng. Technol. 35 (2012) 1346–1358.

[18] P. Sobieszuk, R. Pohorecki, P. Cygański, M. Kraut, F. Olschewski, Marangoni effect in a falling film microreactor, Chem. Eng. J. 164 (2010) 10–15.

[19] K. Warmuziński, J. Buzek, J. Podkański, Marangoni instability during absorption accompanied by chemical reaction, Chem. Eng. J. Biochem. Eng. J. 58 (1995) 151–160.

[20] J. Buzek, J. Podkański, K. Warmuziński, The enhancement of the rate of absorption of CO2 in amine solutions due to the marangoni effect, Energy Convers. Manage. 38 (1997) S69–S74.

[21] C. Heine, K. Kupferschläger, S. Stapf, B. Blümich, NMR velocimetry of falling liquid films, J. Magn. Reson. 154 (2002) 311–316.

[22] T.H. Rehm, C. Berguerand, S. Ek, R. Zapf, P. Löb, L. Nikoshvili, L. Kiwi-Minsker, Continuously operated falling film microreactor for selective hydrogenation of carbon–carbon triple bonds, Chem. Eng. J. 293 (2016) 345–354.

[23] E.V. Rebrov, T. Duisters, P. Löb, J. Meuldijk, V. Hessel, Enhancement of the liquid-side mass transfer in a falling film catalytic microreactor by in-channel mixing structures, Ind. Eng. Chem. Res. 51 (26) (2012) 8719–8725, http://dx.doi.org/10.1021/ie301058h.

[24] A. Cantu-Perez, M. Al-Rawashdeh, V. Hessel, A. Gavriilidis, Reaction modelling of a microstructured falling film reactor incorporating staggered herringbone structures using eddy diffusivity concepts, Chem. Eng. J. 227 (2013) 34–41, IMRET 12: Proceedings of the Twelfth International Conference on Microreaction Technology.

[25] N. Steinfeldt, N. Kockmann, Experimental and numerical characterization of transport phenomena in a falling film microreactor with gas-liquid reaction, Ind. Eng. Chem. Res. 59 (2020) 4033–4047.

[26] J.-N. Tourvieille, F. Bornette, R. Philippe, Q. Vandenberghe, C. de Bellefon, Mass transfer characterisation of a microstructured falling film at pilot scale, Chem. Eng. J. 227 (2013) 182–190, IMRET 12: Proceedings of the Twelfth International Conference on Microreaction Technology.

[27] C.L. Dumoulin, S.P. Souza, R.D. Darrow, N.J. Pelc, W.J. Adams, S.A. Ash, Simultaneous acquisition of phase-contrast angiograms and stationary-tissue images with Hadamard encoding of flow-induced phase shifts, J. Magn. Reson. Imaging 1 (1991) 399–404.

[28] G.C. Saliba, J.G. Korvink, J.J. Brandner, Magnetic resonance velocimetry reveals secondary flow in falling films at the microscale, Phys. Fluids 36 (7) (2024) 071705, arXiv:https://pubs.aip.org/aip/pof/article-pdf/doi/10.1063/5.0214609/20033250/071705_1_5.0214609.pdf.

[29] E. Fukushima, Nuclear magnetic resonance as a tool to study flow, Annu. Rev. Fluid Mech. 31 (1999) 95–123.

[30] C.J. Elkins, M.T. Alley, Magnetic resonance velocimetry: Applications of magnetic resonance imaging in the measurement of fluid motion, Exp. Fluids 43 (2007) 823–858.

[31] M.A. Bernstein, K.F. King, X.J. Zhou, Chapter 15 - angiographic pulse sequences, in: M.A. Bernstein, K.F. King, X.J. Zhou (Eds.), Handbook of MRI Pulse Sequences, Academic Press, Burlington, 2004, pp. 648–701.

[32] M. Al-Rawashdeh, V. Hessel, P. Löb, K. Mevissen, F. Schönfeld, Pseudo 3-D simulation of a falling film microreactor based on realistic channel and film profiles, Chem. Eng. Sci. 63 (2008) 5149–5159.

[33] A.D. Anastasiou, C. Makatsoris, A. Gavriilidis, A.A. Mouza, Application of micro-PIV for investigating liquid film characteristics in an open inclined microchannel, Exp. Therm Fluid Sci. 44 (2013) 90–99.